

# RXFOOD: Plug-in RGB-X Fusion for Object of Interest Detection

Jin Ma<sup>†</sup>, Jinlong Li<sup>†</sup>, Qing Guo, Tianyun Zhang, Yuewei Lin\*, Hongkai Yu\*

**Abstract**—The emergence of different sensors (Near-Infrared, Depth, etc.) is a remedy for the limited application scenarios of traditional RGB camera. The RGB-X tasks, which rely on RGB input and another type of data input to resolve specific problems, have become a popular research topic in multimedia. A crucial part in two-branch RGB-X deep neural networks is how to fuse information across modalities. Given the tremendous information inside RGB-X networks, previous works typically apply naive fusion (e.g., average or max fusion) or only focus on the feature fusion at the same scale(s). While in this paper, we propose a novel method called RXFOOD for the fusion of features across different scales within the same modality branch and from different modality branches simultaneously in a unified attention mechanism. An Energy Exchange Module is designed for the interaction of each feature map’s energy matrix, who reflects the inter-relationship of different positions and different channels inside a feature map. The RXFOOD method can be easily incorporated to any dual-branch encoder-decoder network as a plug-in module, and help the original backbone network better focus on important positions and channels for object of interest detection. Experimental results on RGB-NIR salient object detection, RGB-D salient object detection, and RGB-Frequency image manipulation detection demonstrate the clear effectiveness of the proposed RXFOOD.

**Index Terms**—RGB-X, fusion, object of interest detection

## I. INTRODUCTION

WITH the rapid development of different types of sensors, e.g. RGB camera, Depth, Near-infrared (NIR) etc., human beings are able to acquire various data from the surrounding world now. Each data source provides us a unique perspective of real world, for example, RGB camera delivers colored image by capturing light in red, green, and blue wavelengths, Depth sensor determines the range of an object or a surface to the sensor [65], NIR spectrum contains the material properties of samples that can be used for characterizing objects [47]. These different types of data are complementary to each other, and give us a more comprehensive understanding of captured scene for multimedia research and applications.

The Fig. 1(a) shows three multimedia applications for the RGB-X Object of Interest (OoI) Detection task, where object of interest can be anything that we want to distinguish from others. (1) The RGB image is sometimes vulnerable to light

condition, thus does not contain enough useful information in dark environment, while near-infrared (NIR) can still satisfy visual recognition purpose for salient object detection. (2) In addition, the depth image could assist the RGB images to localize the salient object by giving the extra depth cue. (3) It might be hard to distinguish the tampered region relying only on RGB information, but the Frequency information could be beneficial for the image manipulation detection task. Based on these facts, recent deep learning based neural networks take advantage of multiple data modalities in order to overcome the bias of single data source [47], [32], [51]. In this paper, we denote these deep neural networks for RGB-X OoI as RGB-X encoder-decoder networks, where X represents any type of modality data that is complementary to RGB image and is able to serve as another input data.

The key point in RGB-X networks is how to fuse these two types of modality data for better performance. The fusion process can generally take place at three stages: early fusion [36], [46], [39], intermediate fusion [5], [36], [56], and late fusion [8], [22]. Early fusion combines the RGB and X input together as one single input for network, the intermediate fusion aims to fuse feature representations in the middle layers, and the late fusion makes a unified prediction based on two raw predictions. Despite the simplicity of early fusion and late fusion, their performance is inferior due to the lack of information interactions [5], so the intermediate fusion is a more popular and effective approach. Previous RGB-X related works typically apply naive fusion [47] (e.g., average or max fusion) or only focus on the feature fusion at the same scale(s) [32]. Recent works take multi-scale features into consideration. Multi-scale features (or feature pyramid) have been demonstrated to be helpful for image perception [31] by exploiting features from different scales. Current UNet [44]-like architectures typically use multi-scale features as the guidance for corresponding scales in decoder. *Unlike other works that consider each scale of the multi-scale features separately, this paper aims to design a fusion method that can fuse features across different scales within the same modality branch and from different modality branches simultaneously in a unified attention mechanism.* This module is a flexible plug-in method that can be applied into different RGB-X networks.

The attention mechanism can exploit the context relationship among different positions inside an input [49], then produce a reformulated but more powerful representation for that input. Inspired by the attention mechanism, we propose the RXFOOD fusion method for the OoI detection, which is a flexible and compatible plug-in module with existing two-branch RGB-X encoder-decoder networks. The inter-

Jin Ma, Jinlong Li, Tianyun Zhang and Hongkai Yu are with Cleveland State University, Cleveland, OH, 44115, USA. Qing Guo is with the Centre for Frontier AI Research (CFAR) and Agency for Science, Technology and Research (A\*STAR), Singapore, and the Institute of High Performance Computing (IHPC), Agency for Science, Technology and Research (A\*STAR), Singapore. Yuewei Lin is with Brookhaven National Laboratory, Upton, NY, 11973, USA.

<sup>†</sup> indicates the co-first authors. \* Corresponding authors: Yuewei Lin (e-mail: ywlin@bnl.gov) and Hongkai Yu (e-mail: h.yu19@csuohio.edu).

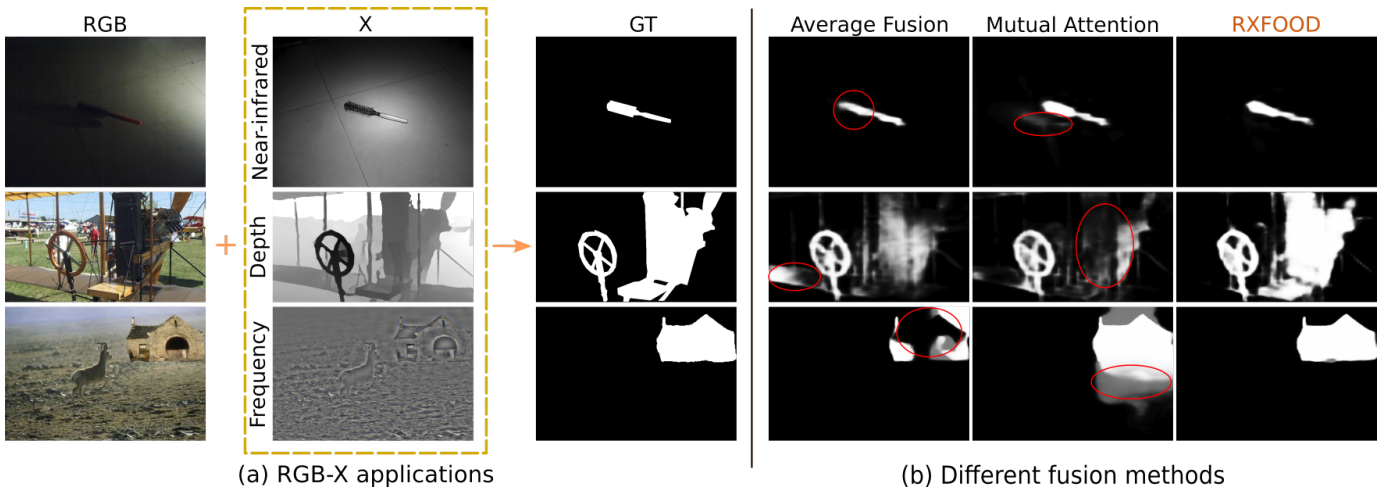


Fig. 1: RGB-X Object of Interest Detection: (a) Diverse multimedia applications, from top to bottom: RGB-NIR salient object detection, RGB-D salient object detection, RGB-Frequency image manipulation detection, whose X inputs are Near-infrared, Depth, and Frequency component respectively. (b) Detection results by different fusion methods: Average fusion, Selective Self-Mutual Attention fusion [32], and the proposed RXFOOD.

relationship of different patches and channels inside an image is an important clue for finding the object of interest, we call this inter-relationship as **energy**, and introduce an Energy Exchange Module that enables the interaction of spatial and channel inter-relationship generated across different scales within the same modality branch and from different modality branches simultaneously. Experimental results show that the fusion process of RXFOOD can enhance features and improve the performance of original backbone network, and it performs better than other comparison fusion methods, as shown in Fig. 1(b). The contributions of our proposed RXFOOD method are summarized as follows.

- We propose a novel method called RXFOOD as RGB-X fusion for the Object of Interest detection, which can fuse the RGB-X information by spatial and channel energy exchange across different scales within the same modality branch and from different modality branches simultaneously.
- The proposed RXFOOD is compatible with existing two-branch RGB-X encoder-decoder networks, which can be easily incorporated with backbone networks as a plug-in module.
- Our intensive experiments on three multimedia tasks (RGB-NIR salient object detection, RGB-D salient object detection, and RGB-Frequency image manipulation detection) demonstrate that the performance of backbone networks could be improved when they are equipped with the proposed RXFOOD.

## II. RELATED WORK

### A. RGB-X Object of Interest Detection

In order to overcome the limitation of single data source, many recent deep learning based methods utilized the additional modality information to help the detection tasks, like depth images [6], [67], [60], [37], thermal infrared

images [58], [10], [48], [66], [54], near-infrared (NIR) images [9], [2], [26], *etc.* Different kinds of image modalities can provide different contributions for computer vision and multimedia tasks. For example, the depth image could assist the RGB images by giving the extra depth information to improve the performance on salient object detection [33], [7], [37], [65] and scene parsing [64]. NIR images contain rich shape and edge information that is useful for detection and segmentation [47], [52], especially when the RGB image is not clear in low light environment. In the field of image manipulation detection, it is hard to distinguish authentic and tampered regions by using only RGB information. While researchers found that they may show different traces in the frequency domain [50], [51], so the frequency information is helpful in image manipulation detection task. In this paper, we focus on the information fusion for RGB-X object of interest detection, where X can be any type of modality data.

### B. RGB-X Fusion

The fusion strategies for combining information from RGB branch and X branch can be roughly divided into three categories: early fusion [43], [19], [35], intermediate fusion [6], [61], [60], [28], and late fusion [17], [22], [67]. Despite the simplicity of early fusion and late fusion, recent state-of-the-art methods typically choose the intermediate representations for fusion due to its high performance on corresponding tasks [56], [16], [62]. Multi-scale features are also important during the fusion process since they can exploit information from different scales. For example, [23] fuses multi-scale features from RGB and NIR for reflection removal. [29] proposes a cross-modal weighting strategy for fusion by using three interaction modules for low-, middle- and high-level features. [20] proposes a siamese network for RGB-D saliency detection by using joint learning and densely cooperative fusion. However, previous fusion methods focus on either the calibrated fusion of each single-scale feature

independently in a cascade manner across modality or the multi-level information fusion within single modality. While in this paper, we aim to propose a plug-in simultaneous fusion method for features across different scales within the same modality branch and from different modality branches in a unified framework.

### C. Attention Mechanism

Attention mechanism is introduced to deep learning inspired by human cognitive nature that people tend to pay attention to specific parts rather than entire scope when perceiving information [11]. By combing the attention module with a deep learning network, the model can focus on valuable information from input, just like human being, so it has been widely applied in various computer vision and multimedia tasks [12], [21], [24], [25], [34], [53], [18]. For example, self-attention mechanism [49] can draw global dependencies between a group of inputs, which can be applied in image generation [57], [38], image classification [53], [30]. Dual attention [18] exploit the long range correlation in spatial and channel dimension. Selective self-mutual attention(S<sup>2</sup>MA) [32] is designed to fuse the features from two different modalities. Our RXFOOD method is also inspired by attention mechanism, whose unique purpose is to fuse features across different scales within the same modality branch and from different modality branches via spatial and channel energy exchange.

## III. METHODOLOGY

### A. RXFOOD Overview

In this section, we introduce the proposed RXFOOD method. Our motivation is that the feature representations from different branches and different scales are complementary to each other, thus the information fusion can help reinforce each feature representation, and improve the network performance. By considering each feature map  $F \in \mathbb{R}^{W \times H \times C}$  as a system contains  $WH$  elements  $\{\alpha_i \in \mathbb{R}^C, i = 1, 2, \dots, WH\}$ , we can compute a spatial-wise similarity matrix with shape  $WH \times WH$  that reflects the inter-relationship (similar or not) of each pair of elements inside the system. In Markov Random Fields (MRF) [3], [4] and the Densely-connected MRF [59] research, the similarity between pairwise elements in MRF can be modeled as energy terms to describe system status. Inspired by their idea, we believe that the spatial-wise similarity matrix ( $WH \times WH$ ) could reflect the system spatial status, so we name it as the **spatial energy** of a feature map based system in this paper. Similarly, we can compute the channel-wise similarity matrix ( $C \times C$ ) as **channel energy** of a feature map based system, which represents the system channel status. These two energy matrices provide clues for finding important spatial positions and channels in object of interest detection, so we develop the proposed RXFOOD method based on energy fusion, which is different from the energy minimization in MRF related works.

As illustrated in Fig. 2, an encoder-decoder backbone network is applied to RGB input and X input respectively with separate parameters. The encoder stage progressively down-samples the resolution of input data, and map input into feature

representations of different scales. The decoder stage takes the feature representations from encoder as input, then make final prediction. Skip connections between encoder and decoder are commonly used approach to make use of multiscale features. Our plug-in RXFOOD method takes multiscale features from two encoders as input, then outputs their fused counterpart features. For example, given the multiscale features extracted by a backbone network from RGB image as  $\{F_{rgb}^1, F_{rgb}^2, \dots, F_{rgb}^n\}$ , and from X image as  $\{F_x^1, F_x^2, \dots, F_x^n\}$ , where  $n$  is the number of scales, and each feature has its own perceptive field. Then the input for our RXFOOD method are these features from different branches and different scales, and the output after fusion are their counterparts  $\{\hat{F}_{rgb}^1, \hat{F}_{rgb}^2, \dots, \hat{F}_{rgb}^n\}$  and  $\{\hat{F}_x^1, \hat{F}_x^2, \dots, \hat{F}_x^n\}$ . These fused features are fed into decoder for final prediction.

There are two components in our RXFOOD method: RGB-X spatial energy fusion, RGB-X channel energy fusion. Next, we will explain these two components in details.

### B. RGB-X Spatial Energy Fusion

**Spatial Energy Computation:** The spatial energy matrix is a by-product of spatial attention mechanism. Given an input feature map  $F \in \mathbb{R}^{W \times H \times C}$  from the encoder, spatial attention exploits the contextual clues among different spatial positions, thus helps the network focus on important regions in object of interest detection. Fig.3(a) shows the general pipeline of spatial attention, first we construct the query  $Q \in \mathbb{R}^{W \times H \times d}$ , key  $K \in \mathbb{R}^{W \times H \times d}$  and value  $V \in \mathbb{R}^{W \times H \times C}$  from input feature map  $F$  by Conv layers, where  $d$  is the number of hidden channels for query and key. Then, we reshape them into query  $Q \in \mathbb{R}^{N \times d}$ , key  $K \in \mathbb{R}^{N \times d}$  and value  $V \in \mathbb{R}^{N \times C}$ , where  $N = W \times H$ . We then compute the **spatial energy** matrix by the following scaled dot-product [49]:

$$\varepsilon = \frac{Q \otimes K^\top}{\sqrt{d}}, \quad (1)$$

where  $\top$  is the transpose operation. This energy matrix reflects the long range inter-dependency clues among all spatial positions. Traditionally, the final output of spatial attention module is computed by the following equation:

$$AS = \alpha \cdot \text{Reshape}(\text{Softmax}(\varepsilon) \otimes V) \oplus F, \quad (2)$$

where  $\alpha$  is a parameter controls the weight of attention, which is a learnable parameter with initial value of 0 in our method. Reshape means to recover the feature to original shape.  $\otimes$  denotes matrix multiplication, and  $\oplus$  denotes element-wise summation. We denote  $AS$  as spatial attention aware feature. The procedure for computing  $\varepsilon$  is marked as hidden step  $h_1$ , and the remaining computation for  $AS$  is marked as hidden step  $h_2$ , as shown in Fig.3(a).

**Spatial Energy Fusion:** As shown in Fig. 3(b), suppose we have the multiscale features  $\{F_{rgb}^1, F_{rgb}^2, \dots, F_{rgb}^n\}$  from RGB branch encoder and  $\{F_x^1, F_x^2, \dots, F_x^n\}$  from X branch encoder, where  $n$  is the total number of scales. Features with lower superscript come from previous layers, so they have larger spatial resolution than those with higher superscript. Our spatial energy fusion method takes these features

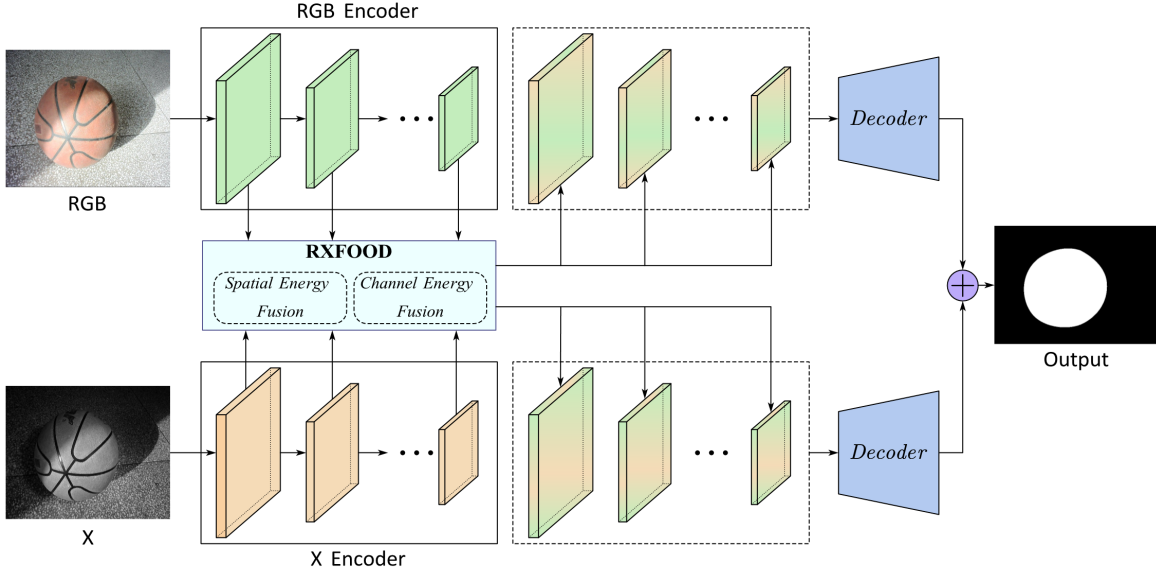


Fig. 2: The pipeline of proposed RXFOOD method. RXFOOD takes multiscale features from different modality encoders as input, then outputs their fused counterparts. These fused multiscale features are fed into decoder for prediction. *Note that the skip connections from multiscale features to decoder are not shown in this figure for simplicity.*

as input, then produces spatial attention aware fused features  $\{AS_{rgb}^1, AS_{rgb}^2, \dots, AS_{rgb}^n\}$  and  $\{AS_x^1, AS_x^2, \dots, AS_x^n\}$ . For each feature  $F_z^i$ , where superscript  $i \in \{1, 2, \dots, n\}$  represents scale and subscript  $z \in \{rgb, x\}$  represents branch, we can compute its corresponding spatial energy matrix  $\varepsilon_z^i$  by changing Eq. 1 to:

$$\varepsilon_z^i = \frac{Q_z^i \otimes (K_z^i)^\top}{\sqrt{d}}, \quad (3)$$

where  $Q_z^i$  and  $K_z^i$  are query and key computed from  $F_z^i$  following the hidden step  $h_1$  as we described above in spatial energy computation. We design an *Spatial Energy Exchange Module* for the fusion of spatial energy matrices from all input, which takes  $\{\varepsilon_{rgb}^1, \varepsilon_{rgb}^2, \dots, \varepsilon_{rgb}^n\}$  and  $\{\varepsilon_x^1, \varepsilon_x^2, \dots, \varepsilon_x^n\}$  as input then output fused energy matrices  $\{\hat{\varepsilon}_{rgb}^1, \hat{\varepsilon}_{rgb}^2, \dots, \hat{\varepsilon}_{rgb}^n\}$  and  $\{\hat{\varepsilon}_x^1, \hat{\varepsilon}_x^2, \dots, \hat{\varepsilon}_x^n\}$ . These fused spatial energy matrices are then utilized to compute the spatial attention aware fused features, by modifying Eq. 2 as:

$$AS_z^i = \alpha \cdot \text{Reshape}(\text{Softmax}(\hat{\varepsilon}_z^i) \otimes V_z^i) \oplus F_z^i, \quad (4)$$

$$i \in \{1, \dots, n\}, z \in \{rgb, x\}.$$

Specifically, Fig. 4 shows the detailed structure of our *Spatial Energy Exchange Module*. As the input spatial energy matrices have different size, first we need to re-scale these energy matrices to the same size. We set the maximum size of all energy matrices as a target size  $S$ , which is the size of  $\varepsilon_{rgb}^1$  and  $\varepsilon_x^1$  in our case. Then upsample all the other energy matrices to the target size  $S$  except  $\varepsilon_{rgb}^1$  and  $\varepsilon_x^1$ . We concatenate the upsampled energy matrices together and feed them into a  $1 \times 1$  Conv layer for information interaction. After information interaction, according to the indexes of those upsampled energy matrices, we downsample corresponding fused energy matrices to the original size. The whole process

of our *Spatial Energy Exchange Module* can be represented as:

$$\{\hat{\varepsilon}_{rgb}^1, \dots, \hat{\varepsilon}_{rgb}^n\}, \{\hat{\varepsilon}_x^1, \dots, \hat{\varepsilon}_x^n\} = SEEM(\{\varepsilon_{rgb}^1, \dots, \varepsilon_{rgb}^n\}, \{\varepsilon_x^1, \dots, \varepsilon_x^n\}), \quad (5)$$

where  $n$  is the number of scales, *SEEM* represents *Spatial Energy Exchange Module*.

### C. RGB-X Channel Energy Fusion

**Channel Energy Computation:** While spatial attention explores the inter-relationship among spatial positions of input, channel attention can help network emphasize channels that are important for object of interest detection, by exploiting inter-dependencies among different channels.

Similarly, the channel energy matrix is the by-product of channel attention, the input feature  $F \in \mathbb{R}^{W \times H \times C}$  is firstly converted to  $F' \in \mathbb{R}^{W \times H \times c}$  by a  $1 \times 1$  Conv layer, where  $c$  is a pre-defined number smaller than  $C$  in order to reduce computational complexity. Then  $F'$  is reshaped to  $f \in \mathbb{R}^{N \times c}$ , this  $f$  is directly used as  $Q, K, V$  to compute the **channel energy** matrix by:

$$\xi = \frac{f^\top \otimes f}{\sqrt{N}}. \quad (6)$$

Then the output of this channel attention module is computed by:

$$AC = \beta \cdot \text{Conv}(\text{Reshape}(\text{Softmax}(\xi) \otimes f)) \oplus F, \quad (7)$$

where  $\beta$  is also a learnable parameter with initial value of 0. Conv is another  $1 \times 1$  Conv layer for recovering number of channels from  $c$  to  $C$ . We denote  $AC$  as channel attention aware feature.

**Channel Energy Fusion:** Just the same way as in spatial energy fusion, given  $F_z^i$  from input of RXFOOD, we first

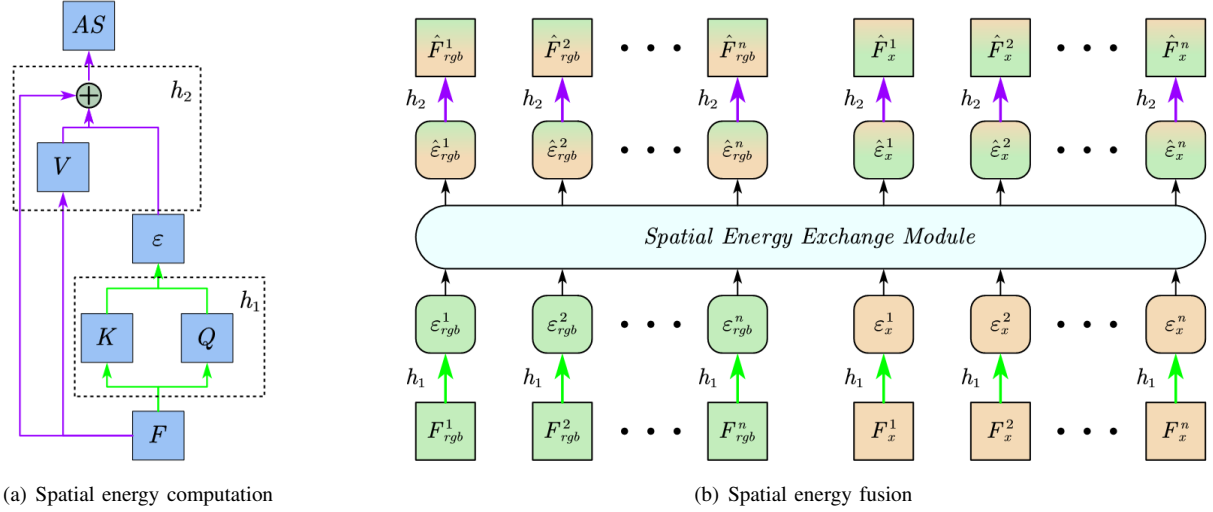


Fig. 3: Illustration of (a) Spatial energy computation, including  $h_1$  and  $h_2$  steps, (b) Our spatial energy fusion method.

compute its corresponding channel energy matrix by changing Eq. 6 to:

$$\xi_z^i = \frac{(f_z^i)^\top \otimes f_z^i}{\sqrt{N}}, \quad (8)$$

where  $f_z^i \in \mathbb{R}^{N \times c}$  is generated from  $F_z^i$ . Then we can feed these channel energy matrices into the *Channel Energy Exchange Module* to get fused output:

$$\{\hat{\xi}_{rgb}^1, \dots, \hat{\xi}_{rgb}^n\}, \{\hat{\xi}_x^1, \dots, \hat{\xi}_x^n\} = CEEM(\{\xi_{rgb}^1, \dots, \xi_{rgb}^n\}, \{\xi_x^1, \dots, \xi_x^n\}), \quad (9)$$

where *CEEM* has the same structure as *SEEM* as shown in Fig. 4 except the input. These fused channel energy matrices are then applied to compute the channel attention aware features by modifying Eq. 7 to:

$$AC_z^i = \beta \cdot \text{Conv}(\text{Reshape}(\text{Softmax}(\hat{\xi}_z^i) \otimes f_z^i)) \oplus F_z^i, \quad (10)$$

$$i \in \{1, \dots, n\}, z \in \{rgb, x\}.$$

After obtaining the spatial attention aware feature  $AS_z^i$  and channel attention aware feature  $AC_z^i$  for each input feature  $F_z^i$ , its fused counterpart feature  $\hat{F}_z^i$  is computed as:

$$\hat{F}_z^i = AS_z^i \oplus AC_z^i, i \in \{1, \dots, n\}, z \in \{rgb, x\}. \quad (11)$$

These fused counterpart features  $\hat{F}_z^i$  will be used in decoder network to replace the original features  $F_z^i$  for final prediction. With the help of the *Spatial Energy Exchange Module* and *Channel Energy Exchange Module*, our RXFOOD method can fuse features across different scales within the same modality branch and from different modality branches simultaneously, and help the backbone network focus more on specific positions and channels that are related to object of interest detection.

#### D. Loss Function

We consider the object of interest detection problem as a pixel-level binary classification problem (either OoI or not), and employ the Binary Cross Entropy (BCE) loss to ensure

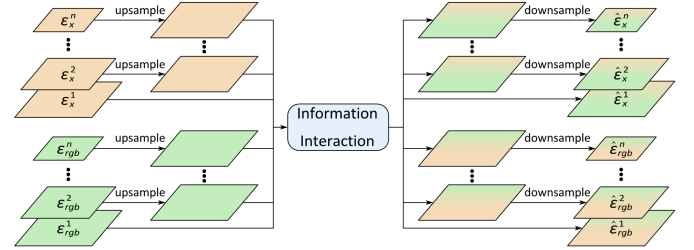


Fig. 4: Illustration of the proposed *Spatial Energy Exchange Module* as shown in Eq. 5. All input spatial energy matrices obtain their fused counterparts after this module.

the correctness of prediction. Let us define the predicted mask as  $X \in \mathbb{R}^{W \times H}$  and the target/ground truth as  $Y \in \mathbb{R}^{W \times H}$ , then the BCE loss is defined as:

$$\mathcal{L}_{BCE} = - \sum_{w=1}^W \sum_{h=1}^H y_{wh} \log x_{wh} + (1 - y_{wh}) \log (1 - x_{wh}). \quad (12)$$

## IV. EXPERIMENTS

This section evaluates several methods on three RGB-X Object of Interest detection tasks, *i.e.*, RGB-N(IR) salient object detection, RGB-D salient object detection and RGB-F (frequency) image manipulation detection.

### A. Experimental Setting

**X branch input:** RGB-N aims to detect salient object by synchronized RGB images and near-infrared images, so the input for X branch is NIR image. While RGB-D aims to detect salient object by synchronized RGB images and depth images, the input for X branch is depth image. For RGB-F image manipulation detection task, we extract the frequency information from RGB images as the input for X branch, the frequency extractor is Frequency-aware Decomposition (FAD) proposed in [41].

**Datasets:** For the RGB-N task, we use the public RGBN-SOD dataset [47] to test our RXFOOD method. This dataset contains 780 synchronized RGB and NIR image pairs, in which 390 pairs are used for training, 78 pairs for validation, and 312 pairs for testing. For the RGB-D task, we use the public ReDWeb-S dataset [33] with 3,179 RGB and depth image pairs, which is divided into a training set with 2,179 image pairs and a testing set with the remaining 1,000 image pairs. For the RGB-F task, we use the public CASIA dataset [13] to test RXFOOD, the training set is CASIA2.0 with 5,123 tampered images and the testing set is CASIA1.0 with 920 tampered images.

**Evaluation metrics:** For RGB-N and RGB-D salient object detection tasks, we use the same metrics Smeasure [14], Emeasure [15], Fmeasure [1], maxF score and MAE [40] as in [47], [32]. For RGB-F image manipulation detection task, we use the area under the ROC curve (AUC) and the maxF score to evaluate the performance, same as the evaluation in [63], [45]. For the MAE metric, the lower the better, while for the others, the higher the better.

**Backbone networks:** As a plug-in, our RXFOOD method can be easily incorporated with other encoder-decoder based networks. For the RGB-N task, we choose its state-of-the-art Two-Branch Network (TBNNet) [47] as our backbone. Specifically, BASNet [42] and CPDNet [55] are employed to implement each branch of TBNNet following its original setting [47], denoted as TBNNet<sub>BAS</sub> and TBNNet<sub>CPD</sub> respectively. While for the RGB-D task, we first adopt the existing two-branch network S<sup>2</sup>MANet [32] as a backbone network, then TBNNet<sub>BAS</sub> and the two-branch Feature Pyramid Networks (FPN) [27] are employed as other backbone networks. Note that S<sup>2</sup>MANet refers to the whole network in [32], while S<sup>2</sup>MA indicates only the Selective Self-Mutual Attention module in their work. As for RGB-F task, we employ TBNNet<sub>BAS</sub> and the two-branch FPN [27] as backbone networks. For TBNNet<sub>BAS</sub>, TBNNet<sub>CPD</sub>, and S<sup>2</sup>MANet, we use features from the last three different scales (n=3) of encoder as input for fusion. For FPN, we use all its four scales (n=4) of encoder as input for fusion. This setting is to show that the proposed RXFOOD method is a flexible plug-in to be easily incorporated into different encoder-decoder based backbone networks with the customized number of scales that the user wants.

**Comparison methods:** We choose three intermediate fusion methods for comparison, including simple average fusion (AVG), max fusion (MAX), and selective self-mutual attention (S<sup>2</sup>MA) based fusion [32]. AVG fusion simply computes the average of input features for fusion, while MAX fusion computes the maximum activation of input features. We apply these two simple fusion methods on same scale features and on multiscales independently. S<sup>2</sup>MA is a specifically designed attention for fusion purpose, and we apply it to the last-layer features of encoder by following the same setting in their original paper [32]. *For each task, we only compare these fusion methods on the strongest backbone network (for that task) with the highest maxF score.*

## B. RGB-N Salient Object Detection

We show quantitative experimental results of RGB-N task in Table. I. As we can see from the table, by adding the proposed RXFOOD fusion method to TBNNet<sub>BAS</sub>, the performance in all metrics are improved. Specifically, there is a large improvement of 5.9% in Fmeasure, and 5% in maxF. TBNNet<sub>CPD</sub> is a more powerful backbone network, its performance is higher than TBNNet<sub>BAS</sub> on all metrics. When applying AVG to TBNNet<sub>CPD</sub>, only Fmeasure and MAE performance are slightly improved by 0.88% and 0.1% respectively, the performance in other metrics are even damaged, this phenomenon also happens in MAX. This is because features from different modalities have information disparity, they cannot be directly combined together. These simple fusion methods cannot address this issue. S<sup>2</sup>MA is beneficial for original backbone network, it improves the original backbone network performance on all metrics by over 0.5%. But its performance is still inferior to our RXFOOD method, which obtains the best scores on all metrics. We display two RGB-N qualitative examples in Fig. 5(a) under similar background condition (top) and dark condition (bottom) respectively. We can see our RXFOOD performs better than other fusion methods under these challenging conditions.

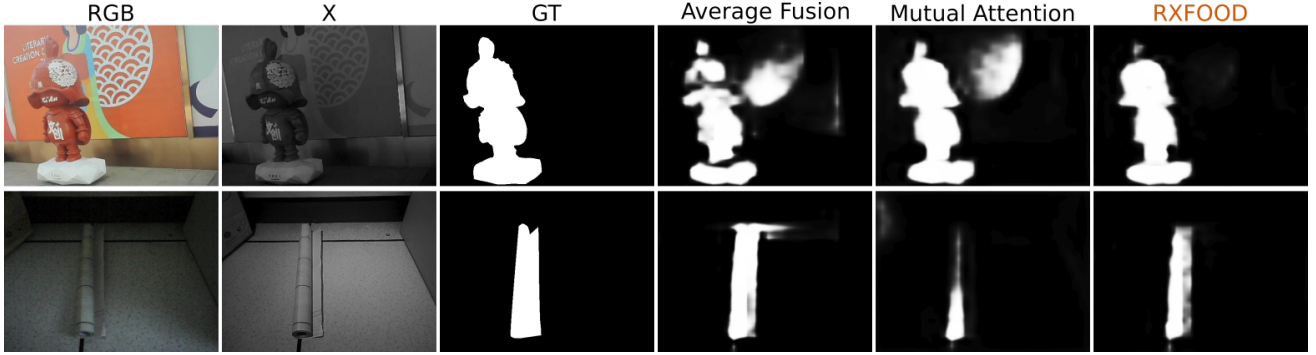
TABLE I: Experimental result comparison on the RGB-N salient object detection task.

Method	Smeasure	Emeasure	Fmeasure	maxF	MAE↓
TBNNet <sub>BAS</sub> [47]	0.8783	0.9122	0.8231	0.8665	0.0496
TBNNet <sub>BAS</sub> +RXFOOD	0.9180	0.9448	0.8821	0.9165	0.0321
TBNNet <sub>CPD</sub> [47]	0.9152	0.9486	0.8741	0.9107	0.0337
TBNNet <sub>CPD</sub> +AVG	0.9120	0.9482	0.8829	0.9064	0.0327
TBNNet <sub>CPD</sub> +MAX	0.9051	0.9380	0.8666	0.8961	0.0365
TBNNet <sub>CPD</sub> +S <sup>2</sup> MA [32]	0.9214	0.9555	0.8888	0.9171	0.0284
TBNNet <sub>CPD</sub> +RXFOOD	<b>0.9232</b>	<b>0.9578</b>	<b>0.8953</b>	<b>0.9212</b>	<b>0.0267</b>

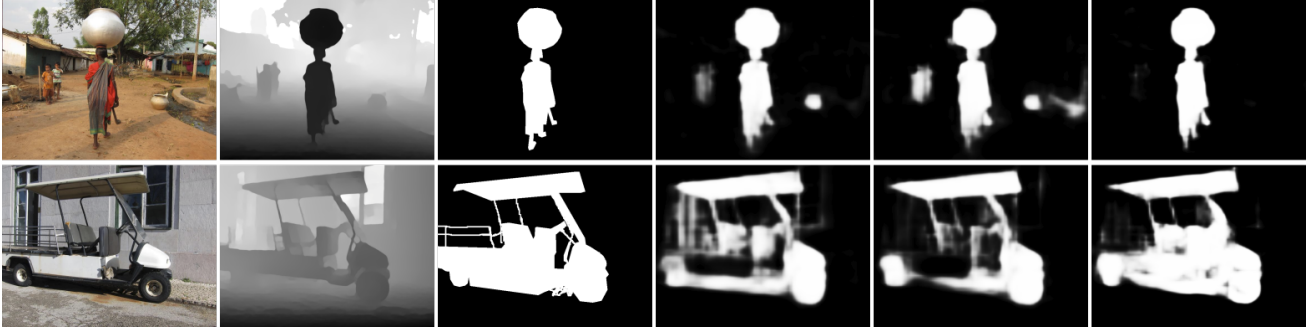
## C. RGB-D Salient Object Detection

The quantitative experimental results of RGB-D task are shown in Table. II. Our RXFOOD method can still improve the performance of backbone networks in this task. For TBNNet<sub>BAS</sub>, the Emeasure is improved from 0.7447 to 0.7572, Fmeasure is improved from 0.6459 to 0.6601. For S<sup>2</sup>MANet [32], we can further improve its performance by adding our RXFOOD fusion method to this dual-branch network. Specifically, the maxF score increases from 0.7302 to 0.7364, and the MAE drops from 0.1346 to 0.1298. The improvement by RXFOOD is more significant in FPN backbone network, with 3.99% in Emeasure, 4.84% in Fmeasure, and 1.57% drop in MAE. Moreover, we can still observe that AVG and MAX fusions are prejudicial to the FPN backbone network in metrics Smeasure and maxF, which demonstrate that these two simple fusion methods are still not good enough in RGB-D applications. S<sup>2</sup>MA does not perform well when applying to FPN, even worse than AVG and MAX fusion. This may due to that mutual attention is designed to fuse information only in the bottleneck stage, but the information in FPN is distributed in feature pyramid. On the contrary, our RXFOOD is still compatible with FPN as a plug-in module. Fig. 5(b) shows

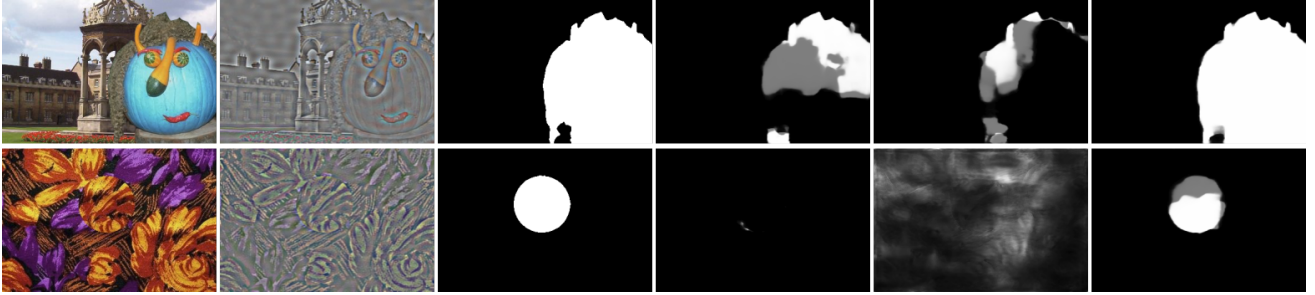




(a) Qualitative examples on RGB-NIR salient object detection. Top: similar background; Bottom: dark condition.



(b) Qualitative examples on RGB-D salient object detection. Top: complex background; Bottom: similar background.



(c) Qualitative examples on RGB-Frequency image manipulation detection. Top: splicing; Bottom: copy-move.

Fig. 5: Qualitative results on three RGB-X Object of Interest detection tasks. From left to right: RGB images, X input images, ground truth, average fusion results, S<sup>2</sup>MA [32] results, and our RXFOOD results.

two examples on RGB-D task, comparing with other fusion methods, our RXFOOD can make more precise predictions.

TABLE II: Experimental result comparison on the RGB-D salient object detection task.

Method	Smeasure	Emeasure	Fmeasure	maxF	MAE↓
TBNet <sub>BAS</sub> [47]	0.7506	0.7447	0.6459	0.7411	0.1367
TBNet <sub>BAS</sub> +RXFOOD	0.7629	0.7572	0.6601	0.7483	0.1284
S <sup>2</sup> MANet [32]	0.7539	0.7704	0.6955	0.7302	0.1346
S <sup>2</sup> MANet+RXFOOD	0.7595	0.7781	0.7023	0.7364	0.1298
FPN [27]	0.7716	0.7640	0.6791	0.7563	0.1271
FPN+AVG	0.7697	0.7712	0.6943	0.7531	0.1234
FPN+MAX	0.7665	0.7861	0.7091	0.7520	0.1216
FPN+S <sup>2</sup> MA [32]	0.7630	0.7671	0.6870	0.7432	0.1260
FPN+RXFOOD	<b>0.7735</b>	<b>0.8039</b>	<b>0.7275</b>	<b>0.7610</b>	<b>0.1114</b>

#### D. RGB-F Image Manipulation Detection

Table. III shows experimental results of RGB-F task. When applying RXFOOD to FPN, the maxF score is improved from 0.3796 to 0.4019, and AUC is improved from 0.7601 to 0.7884. The TBNet<sub>BAS</sub> obtains higher maxF score than FPN, but lower AUC score, because these two metrics are sometimes not positively correlated, where the similar mismatch was reported in the previous work [51]. The AVG can improve maxF from 0.3960 to 0.4114, AUC from 0.6974 to 0.7022, while MAX can only improve the AUC score to 0.7024. S<sup>2</sup>MA can improve the maxF score to 0.4127 and AUC score to 0.7085. When applying our RXFOOD method to TBNet<sub>BAS</sub>, we get the best maxF 0.4380 and AUC 0.7273, comparing with other fusion methods. There are two types of manipulation in testing set, splicing and copy-move, we show one qualitative example for each manipulation type respectively in Fig. 5(c). The top row is an splicing example where RXFOOD performs

much better than other two fusion methods. The bottom row is a difficult copy-move case for all fusion methods, but our RXFOOD can still find the location of indistinguishable tampered region.

TABLE III: Experimental result comparison on the RGB-F image manipulation detection task.

Method	maxF	AUC
FPN [27]	0.3796	0.7601
FPN+RXFOOD	0.4019	<b>0.7884</b>
TBNet <sub>BAS</sub> [47]	0.3960	0.6974
TBNet <sub>BAS</sub> +AVG	0.4114	0.7022
TBNet <sub>BAS</sub> +MAX	0.3901	0.7024
TBNet <sub>BAS</sub> +S <sup>2</sup> MA [32]	0.4127	0.7085
TBNet <sub>BAS</sub> +RXFOOD	<b>0.4380</b>	0.7273

### E. Ablation Study

In order to study the benefits of fusion for multiscales and different modality branches, we conduct ablation study on RGB-N salient object detection task by using TBNet<sub>CPD</sub> as backbone network. Our RXFOOD can be modified to accept single scale features  $\{F_{rgb}, F_x\}$  as input, then we apply it to the last layer features from encoder as in S<sup>2</sup>MANet [32], and denote it as SF (single scale fusion). We also apply SF to multiscale features  $\{F_{rgb}^1, F_x^1\}, \{F_{rgb}^2, F_x^2\}, \dots, \{F_{rgb}^n, F_x^n\}$  independently, and denote it as MSF (multiple single scale fusion). Besides, S<sup>2</sup>MA [32] is also applied to multiscale features independently in order to study its performance on multiscale fusion, which is denoted as MMA (multiple mutual attention). Table. IV shows experimental results for ablation study. As we can see from this table, although S<sup>2</sup>MA is able to improve the original TBNet<sub>CPD</sub>, its multiscale version MMA performs even worse than original TBNet<sub>CPD</sub>. This indicates Mutual Attention is not suitable for the fusion of multiscale features. The TBNet<sub>CPD</sub>+SF slightly improves the performance of original TBNet<sub>CPD</sub>, showing that our energy fusion idea is useful even in single scale condition. By extending SF to multiscale, the performance is further improved, and TBNet<sub>CPD</sub>+MSF is competitive with TBNet<sub>CPD</sub>+S<sup>2</sup>MA, with higher performance on S-Mearure, maxF and MAE. Finally, our RXFOOD method achieves the best score on all metrics, showing that the fusion for features across different scales within the same modality branch and from different modality branches is an effective way for improving network performance.

TABLE IV: Ablation study on RGB-N task by using TBNet<sub>CPD</sub>.

Method	Smeasure	Emeasure	Fmeasure	maxF	MAE↓
TBNet <sub>CPD</sub> [47]	0.9152	0.9486	0.8741	0.9107	0.0337
TBNet <sub>CPD</sub> +S <sup>2</sup> MA [32]	0.9214	0.9555	0.8888	0.9171	0.0284
TBNet <sub>CPD</sub> +MMA	0.9045	0.9398	0.8624	0.8940	0.0327
TBNet <sub>CPD</sub> +SF	0.9169	0.9494	0.8778	0.9135	0.0322
TBNet <sub>CPD</sub> +MSF	0.9220	0.9543	0.8851	0.9178	0.0277
TBNet <sub>CPD</sub> +RXFOOD	<b>0.9232</b>	<b>0.9578</b>	<b>0.8953</b>	<b>0.9212</b>	<b>0.0267</b>

### F. Inference Time

Table V shows the average inference time on each image of the whole testing set on the task of RGB-N salient object detection. All experiments are tested on a single NVIDIA 3090 GPU card. As we can see from the table, the inference time of TBNet<sub>BAS</sub> and TBNet<sub>CPD</sub> for a  $256 \times 256 \times 3$  color image are 0.035s and 0.023s respectively. After applying RXFOOD, the inference time is only increased by 0.002s on TBNet<sub>BAS</sub> and 0.004s on TBNet<sub>CPD</sub>. While the time increase of AVG and MAX on TBNet<sub>CPD</sub> is 0.001s, and the time increase of S<sup>2</sup>MA on TBNet<sub>CPD</sub> is 0.002s. Comparing with the inference time of backbone networks, the inference time difference before and after adding our RXFOOD is still trivial.

TABLE V: Average inference time for one  $256 \times 256 \times 3$  color image on the RGB-N task.

Method	Time (s)
TBNet <sub>BAS</sub> [47]	0.035
TBNet <sub>BAS</sub> +RXFOOD	0.037
TBNet <sub>CPD</sub> [47]	0.023
TBNet <sub>CPD</sub> +AVG	0.024
TBNet <sub>CPD</sub> +MAX	0.024
TBNet <sub>CPD</sub> +S <sup>2</sup> MA [32]	0.025
TBNet <sub>CPD</sub> +RXFOOD	0.027

## V. CONCLUSION

In this paper, we proposed a unified feature fusion method RXFOOD for features across different scales within the same modality and from different modality branches simultaneously, while existing works only handle the single-scale branch fusion or single-branch multiscale fusion. The spatial energy and channel energy inside each feature are important clues for finding object of interest in image, since they reflect the inter-relationship among different spatial positions and channels. So we design *Energy Exchange Module* for information exchange by using spatial and channel energy matrices. Our RXFOOD can be easily integrated with any dual-branch encoder-decoder based networks as a plug-in module. Experimental results on three RGB-X object of interest detection tasks demonstrate that the proposed fusion method is quite effective for improving the performance of original backbone networks.

## REFERENCES

- [1] Radhakrishna Achanta, Sheila Hemami, Francisco Estrada, and Sabine Süsstrunk. Frequency-tuned salient region detection. In *IEEE/CVF Conference on Computer Vision and Pattern Recognition*, pages 1597–1604, 2009.
- [2] Masoomeh Aslahishahri, Kevin G Stanley, Hema Duddu, Steve Shirliff, Sally Vail, Kirstin Bett, Curtis Pozniak, and Ian Stavness. From rgb to nir: Predicting of near infrared reflectance from visible spectrum aerial images of crops. In *IEEE/CVF International Conference on Computer Vision*, pages 1312–1322, 2021.
- [3] Yuri Boykov, Olga Veksler, and Ramin Zabih. Fast approximate energy minimization via graph cuts. *IEEE Transactions on Pattern Analysis and Machine Intelligence*, 23(11):1222–1239, 2001.
- [4] Yuri Y Boykov and M-P Jolly. Interactive graph cuts for optimal boundary & region segmentation of objects in nd images. In *IEEE International Conference on Computer Vision*, volume 1, pages 105–112. IEEE, 2001.
- [5] Hao Chen and Youfu Li. Progressively complementarity-aware fusion network for rgb-d salient object detection. In *IEEE/CVF Conference on Computer Vision and Pattern Recognition*, pages 3051–3060, 2018.



- [6] Hao Chen, Youfu Li, and Dan Su. Multi-modal fusion network with multi-scale multi-path and cross-modal interactions for rgb-d salient object detection. *Pattern Recognition*, 86:376–385, 2019.
- [7] Shuhan Chen and Yun Fu. Progressively guided alternate refinement network for rgb-d salient object detection. In *European Conference on Computer Vision*, pages 520–538. Springer, 2020.
- [8] Yanhua Cheng, Rui Cai, Zhiwei Li, Xin Zhao, and Kaiqi Huang. Locality-sensitive deconvolution networks with gated fusion for rgb-d indoor semantic segmentation. In *IEEE/CVF Conference on Computer Vision and Pattern Recognition*, pages 3029–3037, 2017.
- [9] Runmin Cong, Jianjun Lei, Huazhu Fu, Qingming Huang, Xiaochun Cao, and Nam Ling. Hscs: Hierarchical sparsity based co-saliency detection for rgb-d images. *IEEE Transactions on Multimedia*, 21(7):1660–1671, 2018.
- [10] Runmin Cong, Kepu Zhang, Chen Zhang, Feng Zheng, Yao Zhao, Qingming Huang, and Sam Kwong. Does thermal really always matter for rgb-t salient object detection? *IEEE Transactions on Multimedia*, 2022.
- [11] Maurizio Corbetta and Gordon L Shulman. Control of goal-directed and stimulus-driven attention in the brain. *Nature Reviews Neuroscience*, 3(3):201–215, 2002.
- [12] Hao Dang, Feng Liu, Joel Stehouwer, Xiaoming Liu, and Anil K Jain. On the detection of digital face manipulation. In *IEEE/CVF Conference on Computer Vision and Pattern Recognition*, pages 5781–5790, 2020.
- [13] Jing Dong, Wei Wang, and Tieniu Tan. CASIA image tampering detection evaluation database. In *IEEE China Summit and International Conference on Signal and Information Processing*. IEEE, July 2013.
- [14] Deng-Ping Fan, Ming-Ming Cheng, Yun Liu, Tao Li, and Ali Borji. Structure-measure: A new way to evaluate foreground maps. In *IEEE/CVF International Conference on Computer Vision*, pages 4548–4557, 2017.
- [15] Deng-Ping Fan, Cheng Gong, Yang Cao, Bo Ren, Ming-Ming Cheng, and Ali Borji. Enhanced-alignment measure for binary foreground map evaluation. In *International Joint Conference on Artificial Intelligence*, pages 698–704, 2018.
- [16] Deng-Ping Fan, Yingjie Zhai, Ali Borji, Jufeng Yang, and Ling Shao. Bbs-net: Rgb-d salient object detection with a bifurcated backbone strategy network. In *European Conference on Computer Vision*, pages 275–292. Springer, 2020.
- [17] Yuming Fang, Junle Wang, Manish Narwaria, Patrick Le Callet, and Weisi Lin. Saliency detection for stereoscopic images. *IEEE Transactions on Image Processing*, 23(6):2625–2636, 2014.
- [18] Jun Fu, Jing Liu, Haijie Tian, Yong Li, Yongjun Bao, Zhiwei Fang, and Hanqing Lu. Dual attention network for scene segmentation. In *IEEE/CVF Conference on Computer Vision and Pattern Recognition*, pages 3146–3154, 2019.
- [19] Keren Fu, Deng-Ping Fan, Ge-Peng Ji, and Qijun Zhao. JI-dcf: Joint learning and densely-cooperative fusion framework for rgb-d salient object detection. In *IEEE/CVF Conference on Computer Vision and Pattern Recognition*, pages 3052–3062, 2020.
- [20] Keren Fu, Deng-Ping Fan, Ge-Peng Ji, Qijun Zhao, Jianbing Shen, and Ce Zhu. Siamese network for rgb-d salient object detection and beyond. *IEEE Transactions on Pattern Analysis and Machine Intelligence*, 44(9):5541–5559, 2021.
- [21] Sixue Gong, Xiaoming Liu, and Anil K Jain. Mitigating face recognition bias via group adaptive classifier. In *IEEE/CVF Conference on Computer Vision and Pattern Recognition*, pages 3414–3424, 2021.
- [22] Junwei Han, Hao Chen, Nian Liu, Chenggang Yan, and Xuelong Li. Cnns-based rgb-d saliency detection via cross-view transfer and multiview fusion. *IEEE Transactions on Cybernetics*, 48(11):3171–3183, 2017.
- [23] Yuchen Hong, Youwei Lyu, Si Li, Gang Cao, and Boxin Shi. Reflection removal with nir and rgb image feature fusion. *IEEE Transactions on Multimedia*, 2022.
- [24] Ashrafal Islam, Chengjiang Long, Arslan Basharat, and Anthony Hoogs. Doa-gan: Dual-order attentive generative adversarial network for image copy-move forgery detection and localization. In *IEEE/CVF Conference on Computer Vision and Pattern Recognition*, pages 4676–4685, 2020.
- [25] Takashi Isoke, Songjiang Li, Xu Jia, Shanxin Yuan, Gregory Slabaugh, Chunjing Xu, Ya-Li Li, Shengjin Wang, and Qi Tian. Video super-resolution with temporal group attention. In *IEEE/CVF Conference on Computer Vision and Pattern Recognition*, pages 8008–8017, 2020.
- [26] Shuangping Jin, Bingbing Yu, Minhao Jing, Yi Zhou, Jiajun Liang, and Renhe Ji. Darkvisionnet: Low-light imaging via rgb-nir fusion with deep inconsistency prior. In *AAAI Conference on Artificial Intelligence*, volume 36, pages 1104–1112, 2022.
- [27] Alexander Kirillov, Ross Girshick, Kaifeng He, and Piotr Dollár. Panoptic feature pyramid networks. In *IEEE/CVF Conference on Computer Vision and Pattern Recognition*, pages 6399–6408, 2019.
- [28] Gongyang Li, Zhi Liu, and Haibin Ling. Icnct: Information conversion network for rgb-d based salient object detection. *IEEE Transactions on Image Processing*, 29:4873–4884, 2020.
- [29] Gongyang Li, Zhi Liu, Linwei Ye, Yang Wang, and Haibin Ling. Cross-modal weighting network for rgb-d salient object detection. In *European Conference on Computer Vision*, pages 665–681. Springer, 2020.
- [30] Xiang Li, Wenhai Wang, Xiaolin Hu, and Jian Yang. Selective kernel networks. In *IEEE/CVF Conference on Computer Vision and Pattern Recognition*, pages 510–519, 2019.
- [31] Tsung-Yi Lin, Piotr Dollár, Ross Girshick, Kaifeng He, Bharath Hariharan, and Serge Belongie. Feature pyramid networks for object detection. In *IEEE Conference on Computer Vision and Pattern Recognition*, pages 2117–2125, 2017.
- [32] Nian Liu, Ni Zhang, and Junwei Han. Learning selective self-mutual attention for rgb-d saliency detection. In *IEEE/CVF Conference on Computer Vision and Pattern Recognition*, pages 13756–13765, 2020.
- [33] Nian Liu, Ni Zhang, Ling Shao, and Junwei Han. Learning selective mutual attention and contrast for rgb-d saliency detection. *IEEE Transactions on Pattern Analysis and Machine Intelligence*, 44(12):9026–9042, 2021.
- [34] Xiaohong Liu, Yongrui Ma, Zhihao Shi, and Jun Chen. Griddehazenet: Attention-based multi-scale network for image dehazing. In *IEEE/CVF International Conference on Computer Vision*, pages 7314–7323, 2019.
- [35] Zhengyi Liu, Song Shi, Quntao Duan, Wei Zhang, and Peng Zhao. Salient object detection for rgb-d image by single stream recurrent convolution neural network. *Neurocomputing*, 363:46–57, 2019.
- [36] Zhihao Liu, Jingzhu Wu, Longsheng Fu, Yaqoob Majeed, Yali Feng, Rui Li, and Yongjie Cui. Improved kiwifruit detection using pre-trained vgg16 with rgb and nir information fusion. *IEEE Access*, 8:2327–2336, 2019.
- [37] Youwei Pang, Xiaoqi Zhao, Lihe Zhang, and Huchuan Lu. Multi-scale interactive network for salient object detection. In *IEEE/CVF Conference on Computer Vision and Pattern Recognition*, pages 9413–9422, 2020.
- [38] Niki Parmar, Ashish Vaswani, Jakob Uszkoreit, Lukasz Kaiser, Noam Shazeer, Alexander Ku, and Dustin Tran. Image transformer. In *International Conference on Machine Learning*, pages 4055–4064. PMLR, 2018.
- [39] Houwen Peng, Bing Li, Weihua Xiong, Weiming Hu, and Rongrong Ji. Rgb-d salient object detection: A benchmark and algorithms. In *European Conference on Computer Vision*, pages 92–109. Springer, 2014.
- [40] Federico Perazzi, Philipp Krähenbühl, Yael Pritch, and Alexander Hornung. Saliency filters: Contrast based filtering for salient region detection. In *IEEE/CVF Conference on Computer Vision and Pattern Recognition*, pages 733–740, 2012.
- [41] Yuyang Qian, Guojun Yin, Lu Sheng, Zixuan Chen, and Jing Shao. Thinking in frequency: Face forgery detection by mining frequency-aware clues. In *European Conference on Computer Vision*, pages 86–103, 2020.
- [42] Xuebin Qin, Zichen Zhang, Chenyang Huang, Chao Gao, Masood Dehghan, and Martin Jagersand. Basnet: Boundary-aware salient object detection. In *IEEE/CVF Conference on Computer Vision and Pattern Recognition*, June 2019.
- [43] Liangqiong Qu, Shengfeng He, Jiawei Zhang, Jiandong Tian, Yandong Tang, and Qingxiong Yang. Rgb-d salient object detection via deep fusion. *IEEE Transactions on Image Processing*, 26(5):2274–2285, 2017.
- [44] Olaf Ronneberger, Philipp Fischer, and Thomas Brox. U-net: Convolutional networks for biomedical image segmentation. In *Medical Image Computing and Computer-Assisted Intervention*, pages 234–241. Springer, 2015.
- [45] Ronald Salloum, Yuzhuo Ren, and C-C Jay Kuo. Image splicing localization using a multi-task fully convolutional network (mfcn). *Journal of Visual Communication and Image Representation*, 51:201–209, 2018.
- [46] Hangke Song, Zhi Liu, Huan Du, Guangling Sun, Olivier Le Meur, and Tongwei Ren. Depth-aware salient object detection and segmentation via multiscale discriminative saliency fusion and bootstrap learning. *IEEE Transactions on Image Processing*, 26(9):4204–4216, 2017.
- [47] Shaoyue Song, Zhenjiang Miao, Hongkai Yu, Jianwu Fang, Kang Zheng, Cong Ma, and Song Wang. Deep domain adaptation based multi-spectral salient object detection. *IEEE Transactions on Multimedia*, 24:128–140, 2020.
- [48] Zhengzheng Tu, Zhun Li, Chenglong Li, Yang Lang, and Jin Tang. Multi-interactive dual-decoder for rgb-thermal salient object detection. *IEEE Transactions on Image Processing*, 30:5678–5691, 2021.
- [49] Ashish Vaswani, Noam Shazeer, Niki Parmar, Jakob Uszkoreit, Llion Jones, Aidan N Gomez, Łukasz Kaiser, and Illia Polosukhin. Attention is all you need. *Advances in Neural Information Processing Systems*, 30, 2017.

- [50] Luisa Verdoliva. Media forensics and deepfakes: an overview. *IEEE Journal of Selected Topics in Signal Processing*, 14(5):910–932, 2020.
- [51] Junke Wang, Zuxuan Wu, Jingjing Chen, Xintong Han, Abhinav Shrivastava, Ser-Nam Lim, and Yu-Gang Jiang. Objectformer for image manipulation detection and localization. In *IEEE/CVF Conference on Computer Vision and Pattern Recognition*, pages 2364–2373, 2022.
- [52] Qi Wang, Guokang Zhu, and Yuan Yuan. Multi-spectral dataset and its application in saliency detection. *Computer Vision and Image Understanding*, 117(12):1748–1754, 2013.
- [53] Xiaolong Wang, Ross Girshick, Abhinav Gupta, and Kaiming He. Non-local neural networks. In *IEEE Conference on Computer Vision and Pattern Recognition*, pages 7794–7803, 2018.
- [54] Junyi Wu, Wujie Zhou, Xiaohong Qian, Jingsheng Lei, Lu Yu, and Ting Luo. Menet: Lightweight multimodality enhancement network for detecting salient objects in rgb-thermal images. *Neurocomputing*, 2023.
- [55] Zhe Wu, Li Su, and Qingming Huang. Cascaded partial decoder for fast and accurate salient object detection. In *IEEE/CVF Conference on Computer Vision and Pattern Recognition*, pages 3907–3916, 2019.
- [56] Jin Zeng, Yanfeng Tong, Yunmu Huang, Qiong Yan, Wenxiu Sun, Jing Chen, and Yongtian Wang. Deep surface normal estimation with hierarchical rgb-d fusion. In *IEEE/CVF Conference on Computer Vision and Pattern Recognition*, pages 6153–6162, 2019.
- [57] Han Zhang, Ian Goodfellow, Dimitris Metaxas, and Augustus Odena. Self-attention generative adversarial networks. In *International Conference on Machine Learning*, pages 7354–7363. PMLR, 2019.
- [58] Qiang Zhang, Nianchang Huang, Lin Yao, Dingwen Zhang, Caifeng Shan, and Jungong Han. Rgb-t salient object detection via fusing multi-level cnn features. *IEEE Transactions on Image Processing*, 29:3321–3335, 2019.
- [59] Ziyu Zhang, Sanja Fidler, and Raquel Urtasun. Instance-level segmentation for autonomous driving with deep densely connected mrfs. In *IEEE Conference on Computer Vision and Pattern Recognition*, pages 669–677, 2016.
- [60] Zhao Zhang, Zheng Lin, Jun Xu, Wen-Da Jin, Shao-Ping Lu, and Deng-Ping Fan. Bilateral attention network for rgb-d salient object detection. *IEEE Transactions on Image Processing*, 30:1949–1961, 2021.
- [61] Jia-Xing Zhao, Yang Cao, Deng-Ping Fan, Ming-Ming Cheng, Xuan-Yi Li, and Le Zhang. Contrast prior and fluid pyramid integration for rgb-d salient object detection. In *IEEE/CVF Conference on Computer Vision and Pattern Recognition*, pages 3927–3936, 2019.
- [62] Xiaoqi Zhao, Youwei Pang, Lihe Zhang, Huchuan Lu, and Lei Zhang. Suppress and balance: A simple gated network for salient object detection. In *European Conference on Computer Vision*, pages 35–51. Springer, 2020.
- [63] Peng Zhou, Xintong Han, Vlad I Morariu, and Larry S Davis. Learning rich features for image manipulation detection. In *IEEE/CVF Conference on Computer Vision and Pattern Recognition*, pages 1053–1061, 2018.
- [64] Wujie Zhou, Enquan Yang, Jingsheng Lei, Jian Wan, and Lu Yu. Pgdnet: Progressive guided fusion and depth enhancement network for rgb-d indoor scene parsing. *IEEE Transactions on Multimedia*, 2022.
- [65] Wujie Zhou, Yun Zhu, Jingsheng Lei, Jian Wan, and Lu Yu. Ccafnet: Crossflow and cross-scale adaptive fusion network for detecting salient objects in rgb-d images. *IEEE Transactions on Multimedia*, 24:2192–2204, 2021.
- [66] Wujie Zhou, Yun Zhu, Jingsheng Lei, Rongwang Yang, and Lu Yu. Lsnet: Lightweight spatial boosting network for detecting salient objects in rgb-thermal images. *IEEE Transactions on Image Processing*, 2023.
- [67] Chunbiao Zhu, Xing Cai, Kan Huang, Thomas H Li, and Ge Li. Pdnet: Prior-model guided depth-enhanced network for salient object detection. In *IEEE International Conference on Multimedia and Expo*, pages 199–204. IEEE, 2019.